IEEE copyright notice

Simulation of Automotive Radar Target Lists using a Novel Approach of Object Representation

Markus Bühren and Bin Yang
Chair of System Theory and Signal Processing
University of Stuttgart, Germany
www.LSS.uni-stuttgart.de

***Abstract*— The development of radar signal processing algorithms for target tracking and higher-level automotive applications is mainly done based on real radar data. A data basis has to be acquired during cost-expensive and time-consuming test runs. For a comparably simple application like the adaptive cruise control (ACC), the variety of significant traffic situations can sufficiently be covered by test runs. But for more advanced applications like intersection assistance, the effort for the acquisition of a representative set of radar data will be unbearable. In this paper, we propose a way of simulating radar target lists in a realistic but computationally undemanding way, which will allow to significantly reduce the amount of real radar data needed.**

I. Introduction

In many signal processing areas, for example in channel estimation in mobile communications, the first step in the development of algorithms is to use simulated input data, for example a pseudo-random sequence of bits, and a simulated system like a multipath Rayleigh fading channel. As the model for the transmission channel is simple but close to reality, algorithms can be designed based on simulations. Real measurements are only needed in the final design phase for refinement and verification.

In contrast to this, the development of algorithms in the area of automotive radar signal processing is directly done with the real data itself, which has two major disadvantages. The first disadvantage is that the acquisition of measurement data is both costly and time consuming. While situations on a highway, which are of interest for systems like the adaptive cruise control, are comparably simple to create, scenarios in inner-city environments are of a much higher-dimensional variety. The aim of the presented simulation is a vast reduction in the data acquisition effort.

The second problem when using real data is the performance evaluation of algorithms. In the example of channel estimation given above, the estimated channel impulse response can easily be compared to the known, i.e. simulated, channel impulse response. When directly using real input data, there is no exact reference at all. Algorithms can only be evaluated qualitatively by the time-consuming sight of lots of test scenarios. With simulated radar signals, error measures can easily be computed and algorithms can be evaluated quantitatively.

The reason why engineers in the area of radar signal processing are nevertheless working solely with real data is that the simulation of radar signals is much more complex than the simulation of signals and systems in many other areas. On the one hand, the input data of the system itself is much more complex. Where we have a sequence of bits in mobile communications, the "input data" of the radar system are the positions and shapes of all reflecting objects illuminated by the radar sensor, i.e. other vehicles and obstacles. On the other hand, while the channel in a communication system can often simply be represented by an LTI-system and its impulse response, the "channel" in the radar system, which transforms the above-mentioned "input data" into a radar target list, is of a much higher complexity.

Our simulation of radar signals is aimed to serve as a tool for the development of radar signal processing algorithms that start with the radar target list as input data, i.e. tracking or data fusion algorithms. By restricting the field of use of the simulation to the development of algorithms of that class, we are able to build a simulation that is much simpler than a finite-element model on the level of Maxwell's equations or a ray-tracing model. Simulating radar signals on a very low level would mean a lot of overhead in terms of implementation effort and computation time, as we are only interested in the higher-level radar target list as the desired simulation output.

The motivation for our new approach are the observations of radar experts and our experience with real automotive radar data. We are abstracting vehicles and obstacles in a very simple but accurate way by a small number of reflection centers, which is sufficiently detailed for a realistic simulation of the data we need. Note that in a simulation which is used as a tool for algorithm development, not every physical effect has to be considered. Effects that will not be especially accounted for in the algorithms do not have to be reproduced. The resulting simulation is computationally very undemanding and able to run nearly in real-time on a standard 3 GHz PC. In contrast, a ray-tracing simulation would need in the order of days for the simulation of a scenario of one minute duration.

In section II, the motivation for the new approach of abstracting vehicles and other objects is presented. With this abstraction and a traffic scene (positions, speeds and heading directions of several objects), an ideal radar target list in terms of distance, angle and relative speed can be computed. The ideal target list is then transformed into a realistic one by applying a specific sensor model, as described in section III. The target list simulation principle is summarized in section IV, before real radar target lists are compared to simulated ones in section V. Possible ways of improving the simulation are finally given in section VI.

II. Vehicle Model

The abstraction of vehicles and objects we are going to present in this section is *not* a detailed grid model consisting of many small elements, but a representation consisting of so-called *point reflection centers* and *plane reflectors*. The motivation for this model is the experience with real radar data from numerous test runs. The main observations are now presented with examples.

In the figures 1(a)-1(d), radar target lists that were recorded on test runs are shown in bird's eye-view of the traffic scene. The observing vehicle (on the left) is a Mercedes S-Class equipped with two Tyco Electronics M/A-Com 24 GHz short range radar sensors (SRR), as described in [1]. The sensors are mounted inside the front bumper, the principal angular coverage $[-35^\circ, 35^\circ]$ is indicated. The positions of the detected targets, determined by the measured distance and relative angle, are shown by stars (left sensor) and circles (right sensor), the measured relative speed is shown by a line with proportional length.

The contour of the target vehicle was inserted manually by inspecting simultaneously recorded laser scanner data.

The basic observations are:

O1. When approaching a vehicle straight to the front (Fig. 1(a)) or from behind, the resulting target positions are lying in the center of the target vehicle front or rear end.
O2. When approaching a vehicle onto one of its corners (Fig. 1(b)), the measured target positions are on the corner of the vehicle.
O3. From short distances (Fig. 1(c)), the wheel houses of the target vehicle appear in the target list.
O4. When a vehicle passes the radar sensor perpendicular (Fig. 1(d), object vehicle moving), the radar targets stay in a fixed position as long as the target vehicle side is in view.

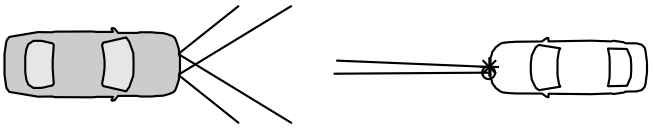

(a) Approaching vehicle straight to the front

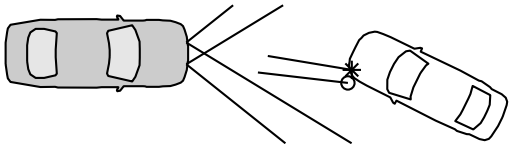

(b) Approaching vehicle onto corner

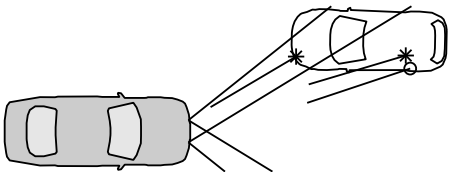

(c) Wheel house reflections

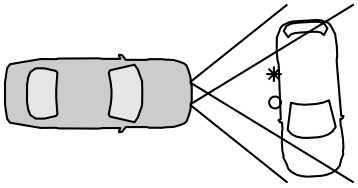

(d) Vehicle passing perpendicular

Fig. 1. Basic observations in real radar data

These basic observations are the motivation for a new approach of abstracting a vehicle by a small number of objects that are simple to describe and easy to handle. The observations O2 and O3 lead to the definition of *point reflection centers*. These are positioned on the four corners and the four wheel houses of the target vehicle. As a wheel house is not visible when the object vehicle is illuminated, for example, from the opposite side, every point reflection center is assigned a visibility function depending on the impinging angle. In Fig. 2, where the shape of an Opel Vectra (the target vehicle in figures 1(a) and 1(b)) is shown from the top, the point reflection centers are at the center points of the eight circle sectors. The circle sectors indicate the region where the visibility function is greater than zero, i.e. the angular region from where they can be detected by a radar sensor.

The observations O1 and O4 show the need for a second type of reflector. As shown in Fig. 2 by thick lines, four *plane reflectors* were placed on the four sides of the target vehicle. The plane reflectors are

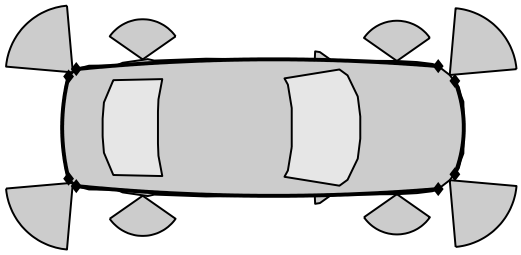

Fig. 2. Vehicle reflection model

represented by circle sectors, or, seen in three dimensions, as a part of the surface of a circular cylinder parallel to the z-axis. Whenever a radar-"ray" hits a plane reflector in perpendicular direction, a reflection point on the circle sector is added as a candidate for an entry in the simulated target list.

To clarify things, in Fig. 3 the determination of visibility for both types of reflectors is illustrated schematically with two different sensor locations. In position 1, the radar sensor illuminates the plane reflector perpendicular but is outside the angular visibility region of the point reflection center, so only the plane reflector can be detected. In position 2 the point reflector can appear in the target list (impinging angle α_2 in the visibility region), but the virtual reflection point on the circle is invalid.

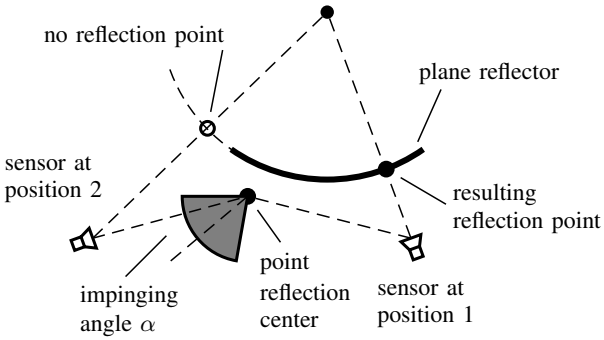

Fig. 3. Visibility evaluation

For both types of reflectors, an important simulation parameter is the radar cross section. This allows the simulation of the radar amplitude and the determination if the returned radar echo is strong enough to cause a detection or not (see section III-B).

The radar cross section of a point reflection center is set to a value proportional to the visibility function of impinging angle α, which is modeled to decrease at the edges of the angular visibility area. In contrast to this, the radar cross section of a plane reflector is set to a constant value.

In each case, reasonable values for the radar cross section have to be derived by inspection of real radar data. Different kinds of planes, for example vehicle front end, rear end and side, will all result in a radar echo of different amplitude. As well, the amount of radar echo to be expected from the wheel houses will differ from vehicle to vehicle. In Fig. 2, the radius of the circle sectors is proportional to the radar cross sections of the corresponding point reflection centers.

With this concept of point reflection centers and plane reflectors, vehicles as well as simpler objects (e.g. reflecting poles, guide boards) and more complicated objects (e.g. trucks) can sufficiently be modeled. In all cases, the necessary parameters have to be derived by inspecting real radar data. The effort for the collection of real data, however, is much smaller in comparison to the usual way, where the algorithm development is done solely based on real data.

III. Sensor model

The vehicle representation was the first part of the model that transforms the positions and shapes of surrounding objects into a radar target list. From the information about the position of the radar sensor and the positions of the reflection centers, an ideal target list in terms of distance, angle and relative speed can be computed by means of geometric considerations. This ideal target list is independent of the particular sensor in use. In this section, the necessary steps to turn the ideal target list into a sensor-specific, realistic target list is explained. All details refer to the SRR radar sensors in [1] as mentioned before. Please note that, as we do not have detailed information about the sensor-internal processing, we have to make assumptions and approximations in several places.

A. Measurement errors in distance and relative speed

Based on the observations of measured data, it can be said that errors in measuring distance and relative speed can sufficiently be simulated by adding pseudo-random white Gaussian noise of appropriately chosen variance to the computed ideal values. These variances and their dependence on range and impinging angle can be derived by inspection of sets of real data. Fig. 4 shows as an example the histogram of the measured distances with a corner reflector as the target, along with a fitted Gaussian probability density curve (the measured distance values are quantized to 1cm).

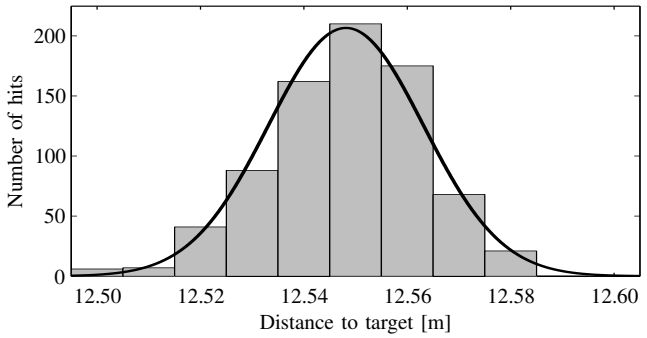

Fig. 4. Histogram of distance measurements

The histogram of the relative speed measurements in the same data set looks similarly Gaussian distributed and is thus omitted here.

B. Simulation of the radar amplitude

In Fig. 5 the measured radar amplitude of a test run where the observing vehicle approached the front of an Opel Vectra is shown. The amplitude is plotted over the distance to the target. As we want to examine only the influence of the front plane reflector of the object vehicle here, we have displayed only those detections with the minimum distance in every cycle. Further, detections with a measured distance greater than that in the last cycle were ignored. This masks the influence of other reflection centers as well as the influence of multiple back-and-forth reflections between the observing vehicle and the object (see section V, Fig. 13(b)).

Note that the well-known $1/R^4$-law for the radar amplitude depending on the distance can not be observed in Fig. 5. This is due to the rapidly changing radar cross section at small distances. In fact, the amplitude level (in dB) shows – in a coarse approximation – a linear decrease over the target distance (about $-0.75\mathrm{dB/m}$, indicated by the trend line in Fig. 5). Following this observation, the range-dependent part of the radar amplitude of the front plane reflector of

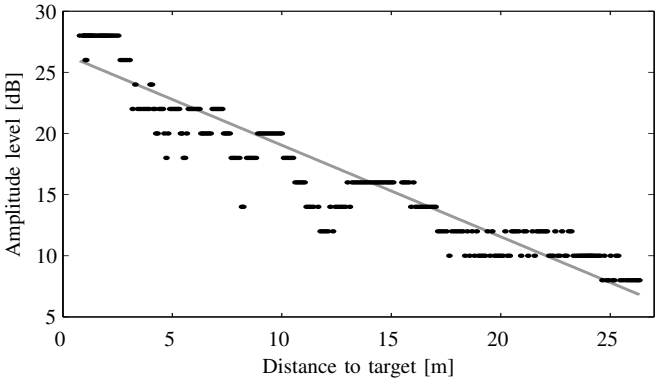

Fig. 5. Radar amplitude of the front of an Opel Vectra

an Opel Vectra, which is used as reference reflector in the following, is simulated as

$$\mathrm{L}\{A^R_{\mathrm{ref}}(R)\} = \left(26.5 - 0.75\frac{R}{\mathrm{m}}\right)\mathrm{dB} \tag{1}$$

where $\mathrm{L}\{A\} = 20\log_{10}|A/A_0|\,\mathrm{dB}$ is the level of the amplitude A in dB related to a reference A_0 and R is the distance to the target. The resulting amplitude also depends on the antenna pattern $A^\phi(\phi)$ (normalized to 1 in the main direction, see section III-D) with the impinging angle ϕ. Thus, the resulting amplitude for the reference reflector is computed as

$$A_{\mathrm{ref}}(R,\phi) = A^R_{\mathrm{ref}}(R)\cdot A^\phi(\phi). \tag{2}$$

By adding pseudo-random noise to the amplitude, the simulation can be made more realistic as misdetections randomly occur for weak targets. An equivalent radar cross section (ERCS) of 1 is arbitrarily assigned to this reference reflector (note that we use normalized numbers because we do not have any information about the relation between the returned amplitude level in dB and the received power in Watt). Other reflection centers are assigned proportional values, which have to be derived by inspection of real radar measurements. Finally, the amplitude generated by an arbitrary reflector k is computed by multiplying the amplitude of the reference target with the equivalent radar cross section of the reflector:

$$A_n(R_n,\phi_n) = A_{\mathrm{ref}}(R_n,\phi_n)\cdot \mathrm{ERCS}_n(\alpha_n) \tag{3}$$

The function $\mathrm{ERCS}_n(\alpha)$ of the impinging angle α includes the visibility function.

The main purpose of the amplitude simulation is the determination if a reflection center is detected by the radar sensor or not. This is done by computing the resulting amplitude for each resolution cell (see next section for the definition of a resolution cell) and comparing it to a threshold. If this amplitude is lower than 6dB (the lowest returned amplitude of any target in our measurements), no target is returned in that resolution cell.

Note that the amplitude in Fig. 5 shows slight decays, e.g. at a distance of about 8m and 12m. These are caused by multipath and interference effects. A multipath-model can be added to the simulation in order to make the amplitude simulation even more realistic.

C. Resolution cells

Until now, all details referred to the case of a single reflection center. In a real radar sensor, not every reflection center will cause its own entry in the target list. Due to the limited resolution of the

radar sensor, all reflection centers in the same resolution cell will be melted into a single target list entry.

The defining dimensions and the size of a resolution cell depend on the radar sensor principle. In our case, a resolution cell is defined in distance and speed; a separation of targets by their relative angle is not possible.

Using a model for the form of the returned radar pulses and the sampling of overlapping pulses in order to reproduce the limited resolution capability would require a number of assumptions. Instead, we are using a simple clustering approach which does not copy the sensor-internal processing but will lead to equal results. The clustering starts with the reflection center with the highest amplitude which defines the center of the first resolution cell. All reflection centers that are inside one nominal resolution in distance and relative speed (we assume 30cm and 0.5m/s) are assigned to this resolution cell. The next resolution cell is then defined by the reflection center with the highest amplitude among the remaining and so on.

An upper threshold for the resulting radar amplitude, A^u_{cell}, is computed as the sum of the amplitudes of all reflection centers in a resolution cell. If this value is lower than the threshold mentioned above, no further computations have to be done for the current cell.

As we expect that reflection centers with a high amplitude $A_n(R_n, \phi_n)$ will have a higher impact on the resulting distance and speed measurement values, d_{cell} and v_{cell}, than those with lower amplitudes, we approximate the superposition of radar energy at the receiving antenna by weighted sums:

$$d_{\text{cell}} = \sum_n d_n w_n \quad , \quad v_{\text{cell}} = \sum_n v_n w_n \tag{4}$$

with

$$w_n = A_n(R_n, \phi_n) / \sum_n A_n(R_n, \phi_n) \tag{5}$$

The estimation of a relative angle ϕ_{cell} for each resolution cell is described in detail in the following section.

D. Simulation of the angle estimation principle

For a realistic simulation of errors in the measured angle, it is inevitable to take the angle estimation principle into account, rather than simply adding pseudo-random noise to the ideal angle. The motivation for this is a particular effect that emerges when there are two or more objects in the same resolution cell but significantly separated in angle. In this case the backscattered radar energy of all objects superimposes at the radar receiver and leads to an erroneous angle estimation. A real data example is shown in Fig. 6; a single detection with erroneous angle can be seen in the center between the two object vehicles. As special care has to be taken for this effect in the target list processing, it should be considered in the simulation as well.

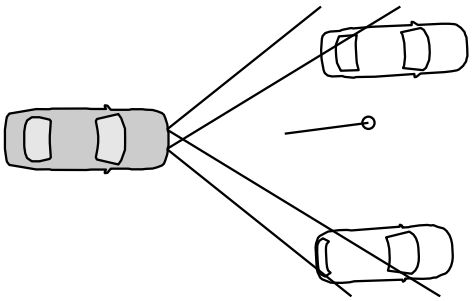

Fig. 6. Angle estimation error in one resolution cell

The basic idea of the angle estimation procedure (monopulse principle) implemented in the sensors under consideration is to use two receive antennas with different antenna patterns (so-called *sum* and *delta* patterns [1], see Fig. 7). The target direction ϕ can then be computed unambiguously from the received combination of amplitudes and phases separately for each resolution cell.

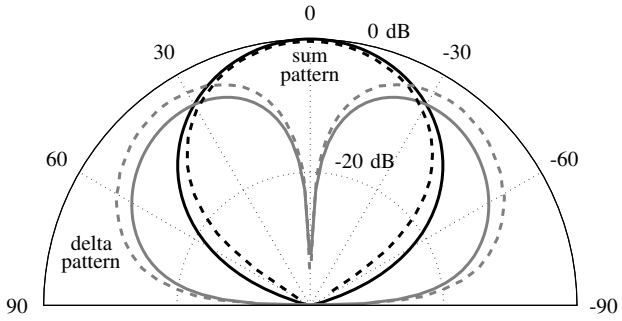

Fig. 7. Antenna patterns of sum and delta beams

The sum and delta patterns in azimuth from [1] (dashed lines in Fig. 7) can be approximated by the antenna patterns of an array of two dipole antennas of length L spaced by a half wavelength λ (solid lines in Fig. 7). For the sum pattern, both dipoles are switched in phase, while a phase shift of π is introduced for the delta pattern. The resulting complex pointers, neglecting factors depending on elevation angle and target distance, are (Σ: sum pattern, Δ: delta pattern) [2]:

$$H_{\substack{\Sigma \\ \Delta}}(\phi) = \text{si}\left(\frac{\pi L}{\lambda}\sin(\phi)\right)\cos(\phi) \cdot \frac{1}{2}\Big(1 \pm \exp\left(j\pi\sin(\phi)\right)\Big) \tag{6}$$

The magnitude of the sum pointer is used as the antenna pattern $A^{\phi}(\phi)$ in equation (2). In connection with equations (1)-(3) and the detection threshold of 6dB, the detection area for different values of the equivalent radar cross section ERCS results as illustrated in Fig. 8 in the top view.

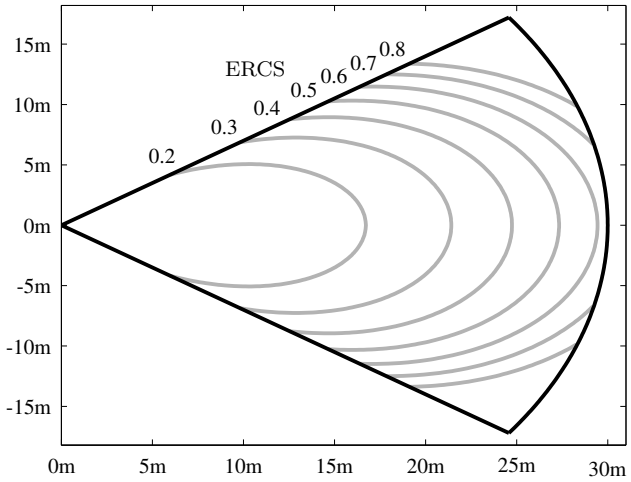

Fig. 8. Visibility area for different ERCS values

The so-called *additive sensing ratio*

$$\text{ASR}(\phi) = \frac{|H_{\Delta}(\phi)| - |H_{\Sigma}(\phi)|}{|H_{\Delta}(\phi)| + |H_{\Sigma}(\phi)|} \tag{7}$$

is a monotonously increasing function of the absolute angle $|\phi|$ and can be inverted by table-lookup or a spline representation. The sign

of the target angle can be determined by the phase difference between sum and delta pulse (see [1] for details).

In the angle computation model, the computed ideal angles of all reflection centers in a specific resolution cell are considered. Using the closed form expression for the antenna patterns (equation (6)), the ideal angles are transformed into pairs of complex pointers corresponding to the two antenna patterns. These pointers are weighted by the distance-dependent part of simulated amplitude, as we expect that a weak target will have less influence on the angle estimation than a strong one. The complex pointers corresponding to the sum and delta pulses of all reflectors in the current resolution cell are then summed up. In order to incorporate angle estimation noise into the sensor model, complex Gaussian pseudo-random noise is added to the resulting two pointers:

$$H_{\text{cell},\frac{\Sigma}{\Delta}} = \sum_n A^R_{\text{ref}}(R_n) \cdot \text{ERCS}_n(\alpha_n) \cdot H_{\frac{\Sigma}{\Delta}}(\phi_n) + \text{Noise} \qquad (8)$$

As the artificial noise is of constant variance while the pointers are weighted by the simulated amplitude, targets with lower amplitude will inherently be subject to higher angle errors, as we would expect in reality. From the resulting two pointers $H_{\text{cell},\Sigma}$ and $H_{\text{cell},\Delta}$, the angle estimation is now straightforward using the additive sensing ratio in equation (7) and the phase information as described in [1]. We found that adding Gaussian noise with an amplitude of -18dB (compared to the unknown reference A_0) results in a standard deviation of the simulated angle measurements similar to that in the corner reflector measurement from Fig. 4.

E. Sensor-internal tracking

In the simulation as described up to this point, the radar target lists of two consecutive time instances are independent of each other. In the real radar data, however, we can clearly observe effects of sensor-internal tracking. This processing step is important to suppress false detections and to smooth the noisy estimations, especially the angle estimations. A trade-off has to be made between the degree of false detection suppression and smoothing on the one hand and the reaction time, i.e. the number of time steps until a true target is approved, on the other hand.

While finding the optimal tracking procedure is a challenging task in the sensor design, building a model of it is much simpler due two reasons: First, we do not have to cope with false detections. Second, while the noise characteristics of the real measurements are fixed and the tracking parameters have to be chosen optimally, in the simulation we can modify both the noise characteristics and the tracking parameters in order to yield realistic results.

We model the sensor-internal tracking using a simple linear Kalman filter approach [3] with the same states as the radar target list entries. The final target list is built from those tracks that were assigned a minimum number of measurements in the past cycles. Tracks are deleted after not being assigned new measurements for several time steps. As the tracking model is still subject to change and improvement, we skip further details here.

IV. Target List Simulation Summary

In this section, the necessary steps from a traffic situation to a realistic target list are summarized. A graph with the hierarchical simulation structure is shown in Fig. 9.

1) Object model database: The reflection center representation of all involved objects in terms of positions, equivalent radar cross sections and visibility functions (for point reflection centers) have to be derived by inspection of real radar data. The choice of these parameters is expected not to be critical and can be done with a moderate amount of measurement data.

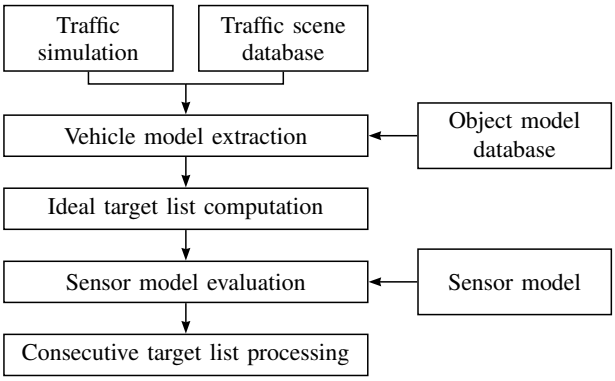

Fig. 9. Hierarchical simulation structure

2) Sensor model: The sensor model includes the specification of the radar sensor in terms of maximum range, angular coverage, resolution and accuracy in distance and relative speed as well as the quantization of the returned measurements. The angle estimation principle with the involved antenna patterns and the sensor-internal tracking algorithm are also part of the sensor model.

3) Traffic simulation/traffic scene database: The exact positions of vehicles and obstacles around the observing vehicle can be generated either by use of a traffic simulation, where the behavior of virtual vehicles is modeled by a so-called microscopic traffic model (see, for example, [4] [5]), or by defining the movement of observer and objects manually for each time step. Both possibilities are realized in our simulation, but will not be discussed in detail here.

4) Vehicle model extraction: In the vehicle model extraction part of the simulation, all objects and vehicles around the observer are dissolved into reflection centers. For each object, it is checked which of its reflectors are in principle visible to the radar sensor.

5) Ideal target list computation: For each reflector, the ideal target list entry in terms of distance, angle and relative speed is computed.

6) Sensor model evaluation: The sum and delta pointers are computed for each reflector and scaled with the simulated amplitude. The reflectors are then partitioned into resolution cells of distance and speed. For each resolution cell, the scaled sum and delta pointers of the corresponding reflectors are summed up. Artificial complex noise is added before the resulting angle is computed. The resulting radar amplitude, distance and relative speed are computed per resolution cell; artificial noise is added to the results. The target list that is formed by the results of all resolution cells in which there was a detection is passed over to the sensor-internal tracking. The states of all approved tracks form the final radar target list that can now be forwarded to consecutive processing algorithms like target tracking and sensor data fusion.

V. Results

Figures 10-13 contain comparisons between real target lists and their simulated counterparts. The observing vehicle is in each case located on the left of the target vehicle. As stated before, the vehicle contours were set manually into the real data scenarios with help of laser scanner data. The same positions and the corresponding object vehicle representation were used to simulate the radar target list in the same scenario. The traces of stars and circles represent the detections of the two sensors in the last ten time instances, while the object vehicle position of the last time step is displayed.

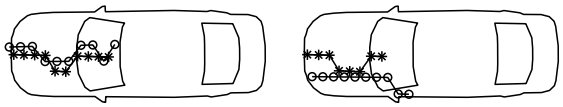

(a) Simulated (b) Real

Fig. 10. Real and simulated data in situation 1

Clearly, real and simulated data show similar characteristics in situation 1 (Fig. 10), where the observer approaches the front of the Opel Vectra. The distance to the target in the last displayed time instance is about 15m. The results are also satisfactory in situation 2, where the observer approached the corner of the same vehicle (Fig. 11, distance about 12.5m).

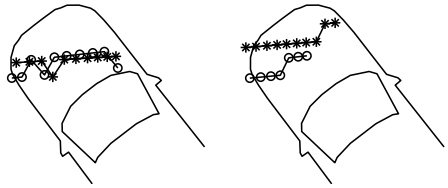

(a) Simulated (b) Real

Fig. 11. Real and simulated data in situation 2

In the next situation in Fig. 12, the distance between observer and target is about 2.8m. The concept of the front plane reflector is very well approved. In the simulated data, the detections around the left side of the target vehicle windshield are missing. These detections with low amplitude only occur at small distances and are presumably caused by non-ideal focusing in elevation direction.

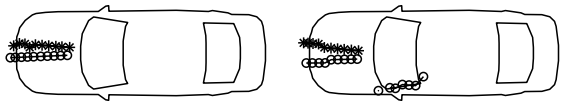

(a) Simulated (b) Real

Fig. 12. Real and simulated data in situation 3

Finally, Fig. 13 shows a single snapshot of a situation that our simulation is not yet capable to reproduce correctly. Observer and target vehicle are standing still with a distance of about 1m. While the front plane reflector model is approved again by the detections on the left, in the real data there are a number of additional detections. These occur because the radar energy that propagates more than one time between object and observing vehicle (multiple back-and-forth reflections) is still strong enough to cause a detection.

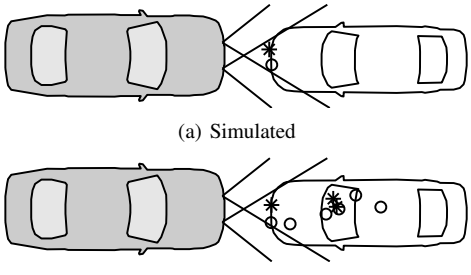

(a) Simulated

(b) Real

Fig. 13. Real and simulated data in situation 4

VI. Outlook and further work

The simulation in its current state is able to generate realistic radar targets lists in the majority of scenarios. By considering some additional effects, the range of possible scenarios can even be expanded.

We have mentioned before that in situations where the distance between radar sensor and object is very small, additional detections are caused by multiple back-and-forth reflections. This effect can be modeled by adding duplicates of existing reflection centers at integer multiples of the measured distance.

Further, a multipath propagation and interference model could be added to enhance the radar amplitude simulation. If the amplitude is only of secondary importance in the consecutive processing algorithms, the current solution is sufficient.

The presented real data sets were recorded in a test site free of any disturbing obstacles, thus misdetections were very rare. In other environments, however, there will be more misdetections due to numerous small reflectors or multiple reflections between different obstacles. As the target list processing algorithms have to cope with those spurious targets, they should also appear in simulated target lists. For the algorithms it will not be important how exactly a misdetection occurred, thus it will be sufficient to add misdetections randomly instead of adding, for example, a sophisticated ray-tracing model for multiple reflections between objects.

VII. Conclusion

We have presented a new simulation principle for automotive radar target lists. By limiting the intended application area of the simulation to the development of target list processing algorithms, we were able to significantly reduce the programming effort as well as the computational load in comparison to a finite-element-like simulation.

Vehicles and obstacles are represented by a small number of point reflection centers and plane reflectors, which are parametrized with aid of a moderate amount of real measurement data. A geometrically computed ideal target list is turned into a realistic one by applying a simplified sensor model and adding artificial noise in different stages.

As we have shown by the results of our simulation, not every detail about the sensor internals is necessary to build a realistic sensor model and to simulate a realistic radar target list. Even if not every physical effect is considered, the simulation is a valuable tool for the development of radar signal processing algorithms.

Acknowledgment

This work was kindly supported by Dirk Linzmeier and Michael Skutek of the DaimlerChrysler AG by providing the opportunity to record the necessary radar measurement data.

References

[1] H. Henftling, D. Klotzbücher, and C. Frank, "Ultra wide band 24GHz sequential lobing radar for automotive applications," in *Proc. Intern. Radar Symposium (IRS)*, Berlin, Germany, Sept. 2005.

[2] C. A. Balanis, *Antenna Theory*. New York, NY: John Wiley & Sons, 1982.

[3] S. S. Blackman, *Multiple-Target Tracking with Radar Applications*. Artech House, 1986.

[4] R. Wiedemann, *Simulation des Straßenverkehrsflusses*. Schriftenreihe des Instituts für Verkehrswesen der Universität Karlsruhe, Heft 8, 1974.

[5] P. G. Gipps, "A model for the structure of lane-changing decisions," *Transportation Research*, vol. 20B, no. 5, pp. 403–414, 1986.